Review

Synthesis of lamp phosphors: facile combustion approach

S. Ekambaram[a,*], K.C. Patil[b], M. Maaza[c]

[a] *Purdue University, Forney Hall of Chemical Engineering, 480 Stadium, Mall Drive, West Lafayette, IN 47907, USA*
[b] *Inorganic and Physicas Chemistry Department, Indian Institute of Science, Bangalore-12, India*
[c] *School of Physics, University of Witwatersrand, Johannesburg, South Africa*

Abstract

This review article is intended to show feasibility of solution combustion process for the synthesis of rare-earth activated insulating materials at low temperature (350–500 °C) and in a very short time (<5 min). Thus, this review starts with combustion synthesis followed by luminescent properties of combustion synthesized tricolour lamp phosphors. Major focuses in red phosphors are effect of calcinations and of impurities on luminescence of Eu^{3+} activated red phosphors. In the Eu^{2+} activated blue phosphor section, effect of activator concentration (Eu^{2+}) and concentration of BaO in $BaO{\cdot}6Al_2O_3$ are studied. In the case of green phosphors, co-doping of Eu^{2+}, Ce^{3+} and Tb^{3+} in $LaMgAl_{11}O_{19}$ is investigated.

Keywords: Combustion; Low temperature; Lamp phosphors

Contents

* Corresponding author. Tel.: +1 765 496 6120; fax: +1 765 494 4050.
E-mail address: s_ekambaram69@hotmail.com (S. Ekambaram).

1. Introduction

Phosphor materials find wide applications ranging from fluorescent lamp to luminescence immunoassay [1]. These materials essentially convert one type of energy into visible radiation and hence, phosphor materials are called optical transducer. They are generally crystalline in nature. Since, the theme of this review article is focused on lamp phosphors, we will be concentrating on phosphor materials used in tricolour lamp. In the fluorescent lamp, phosphor materials convert UV radiation into visible radiation. Lamp phosphors are mostly white in colour and they should not absorb the visible radiation.

Fluorescent lamp is made of glass tube sealed with two ends in which noble gas and Hg vapour are present in 400 and 0.8 Pa pressure, respectively [1]. About 11.5 mg of Hg is used in fluorescent lamp of diameter 30 mm. In the electric discharge Hg atoms are excited to higher energy levels. When they return to ground state it emits 85% 254 nm wave length, 12% 185 nm and 3% in the visible radiation. Phosphor materials coated inside the tube essentially convert 254 and 185 nm wavelengths into visible radiation. Thickness of phosphor materials coated inside the tube is in the order of 20–40 μm. Since phosphors have direct contact with Hg, potential phosphors such as ZnS can not be used because of reaction between Hg and ZnS. Therefore, oxides are used as the hosts for fluorescent lamps.

There are three types of fluorescent lamps available currently and these are halophosphate lamp, tricolour lamp and special de luxe lamp [2]. Among them, tricolour lamp phosphors form a special group. The tricolour lamp phosphors are 60 wt.% Y_2O_3:Eu^{3+}, 30 wt.% $CeMgAl_{11}O_{19}$:Tb^{3+} and 10 wt.% $BaMgAl_{10}O_{17}$:Eu^{2+}, where, Eu^{3+}, Eu^{2+} and Tb^{3+} are activators. In the case of green, non-radiative energy, transfer goes directly from Ce^{3+} to Tb^{3+} and hence, lot of cerium and terbium oxides are required. Therefore, this green phosphor has been replaced by other two green phosphors, viz. (La,Ce)PO_4:Tb^{3+} and (Ce,Gd)MgB_5O_{10}:Tb^{3+}. In these newly developed phosphors, Tb^{3+} is activated via energy migration in the Ce^{3+} and Gd^{3+} sublattice, respectively. Thus, concentration of terbium oxide is reduced and hence, cost of the phosphor is improved [3]. Because of improved lumen output and greater radiation stability of tricolour lamp phosphors over conventional lamp phosphor (linear fluorescent), diameter of the fluorescent lamp could be reduced to 10 mm from 38 mm. This innovation results in Hi-Tech compact fluorescent lamps with various sizes and shapes.

There has been an increasing interest in rare-earth phosphors since 1980 as evidenced from the number of international conferences held [4–8], technical reports [9–24] and reviews [25–35] published. Phosphors activated by rare earth ions exhibit some peculiarities. In the energy level diagram of the rare-earth, luminescence processes often correspond to electronic transitions within the incompletely filled 4f shell, which is extensively shielded from host lattice [2]. Consequently, these phosphors have narrow band spectra which are to a great extent independent of the nature of the host lattice. Because of the low interaction with the crystal field, luminescence quantum yield of phosphors activated with rare earths is often high compared to other phosphors. Quenching occurs only at higher temperatures or higher activator concentrations. Europium (II and III) and terbium are of interest as activators for getting tricolour lamp phosphors.

2. Synthesis of lamp phosphors

2.1. Conventional solid state method

The fluorescent lamps are coated with phosphor by using a suspension of phosphor powder particles. A lamp phosphor is, therefore, needed as a powder. The luminescent activator concentration is of the order of 1–3% (atom percent). Therefore, high quality starting materials and a clean production process are prerequisite for obtaining luminescent materials with a high efficiency.

Because of refractory nature of alumina and rare-earth oxides, conventional synthesis of lamp phosphors requires temperature greater than 1000 °C. Thus, corresponding metal oxides/carbonates are ground well and heated >1000 °C. The mechanism of solid state reactions is diffuse control reaction and hence, repeated grinding and repeated heating are required [36–44]. The controlled atmosphere is necessary to master the valence of the activator (for example Eu^{2+} or Eu^{3+}) and the stoichiometry of the host lattice. Therefore, doping 1–3% of activator in oxide host has been delicate. For example, preparation of Tb^{3+} activated $CeMgAl_{11}O_{19}$ green phosphor has been achieved from a mixture of Al_2O_3, $MgCO_3$, CeO_2 and Tb_4O_7 at 1500 °C, 5 h with small quantities of MgF_2 or AlF_3 as a crystallizing agent [41].

Limitations in synthesis of lamp phosphors by conventional solid state method.

Preparation of single phase compound is difficult by the conventional solid state method. Hence, doping a low con-

centration (of the order of 1–3%) of activator has always been delicate. Thus, the limitations of conventional solid state method are

1. Inhomogeneity of the product.
2. Formation of large particles with low surface area and hence, mechanical particle size reduction is required, which introduces impurity and defects.
3. Presence of defects, which are harmful to luminescence.

The problem of inhomogeneity could be mitigated by the use of non-conventional methods (wet-chemical).

2.2. Wet-chemical methods

Wet-chemical techniques are now available for simple oxide phosphor synthesis such as Eu^{3+} activated Y_2O_3 red phosphor. These techniques [45,46] are defined as techniques which do not comprise of the normal mixing, calcinations and grinding operations. Wet-chemical methods such as co-precipitation [47], sol–gel [48,49], hydrothermal [50], evaporative decomposition [51], reverse micellar [52,53], surface modifier [54] etc. have been employed to synthesize rare-earth activated lamp phosphors. These wet-chemical methods dope rare earth activators uniformly. But, calcination is required to get crystalline (required) phosphors. However, to my knowledge, wet-chemical techniques are not available for the synthesis of complex oxide phosphors (blue and green phosphors). Therefore, we would like to emphasise importance of solution combustion process, for the synthesis of both simple and complex oxide phosphors. In the following section, we deal with solution combustion synthesis and luminescent properties of rare-earth activated lamp phosphors.

2.3. Combustion method

Combustion method [55,56] is yet another wet-chemical method which does not require further calcinations and repeated heating. This method was accidentally discovered in 1988 in Prof. Patil's lab in India. It is an exothermic reaction and occurs with the evolution of heat and light. Such a high temperature leads to formation and crystallization of phosphor materials.

For any combustion, fuel and oxidizer are required. When the mixture of fuel and oxidizer are ignited, combustion takes place. For the combustion synthesis of oxides, metal nitrates are used as oxidizer, and fuels employed are hydrazine based compounds or urea or glycine. Stoichiometric compositions of metal nitrates and fuels are calculated based upon propellant chemistry. Thus, heat of combustion is maximum for O/F ratio 1 [55]. Based on the concepts used in propellant chemistry [55], the elements C, H, V, B or any other metal are considered as reducing elements with valencies 4+, 1+, 5+, 3+ (or valency of the metal ion in that compound), respectively and oxygen is an oxidizer having the valency of 2−. The valency of nitrogen is taken as zero because of its conversion to molecular nitrogen during combustion. Accordingly, the oxidizing (O) and reducing (F) valencies for $M(NO_3)_3$ and oxalyl dihydrazide can be calculated as follows.

$M(NO_3)_3$
1M = 3+
9O = 18−
3N = 0

15−
where, M = Y, Gd, La, Al, Tb, Ce.

Oxalyl dihydrazide, $C_2H_6N_4O_2$(ODH)
2C = 8+
6H = 6+
2O = 4−
4N = 0

10+

The oxidizing and reducing valencies of metal nitrates and fuels used in the combustion synthesis of oxide phosphors are summarized in Table 1. Thus, the stoichiometry for the preparation of Ln_2O_3 where Ln = Y, La and Gd from $Ln(NO_3)_3$:ODH becomes 1:1.5.

The preparation of ytrria using yttrium nitrate and oxalyl dihydrazide (ODH) redox mixture is described below as a representative of all phosphors.

Yttrium nitrate (11.493 g, 0.03 mol) and oxalyl dihydrazide (5.314 g, 0.045 mol) were dissolved in a minimum amount of water in a pyrex dish (100 mm × 50 mm). The pyrex dish was introducted into a muffle furnace (l = 28 cm, b = 17 cm and h = 7 cm) maintained at 400 °C. The solution boils, foams and ignites to burn with flame to yield voluminous, foamy yttria. Flame temperature measured by an optical pyrometer was 1400 °C ± 100 °C. The entire combustion process lasted for about 5 min. The combustion process is self-propagating i.e., once ignited it goes to completion without the supply of additional heat from an external source.

Table 1
Oxidizing and reducing valencies of metal nitrates and fuels

Compound	Oxidizing/Reducing valency
$M(NO_3)_2$	10−
$M(NO_3)_3$	15−
$M(NO_3)_4$	20−
NH_4NO_3	2−
Urea, CH_4N_2O	6+
Carbohydrazide (CH), $CH_6N_4O_2$	8+
Oxalyl dihydrazide (ODH), $C_2H_6N_4O_2$	10+
3-Methyl Pyrazole 5-One (3MP5O), $C_4H_6N_2O$	20+
Diformyl hydrazine (DFH), $C_2H_4N_2O_2$	8+
$Y(N_2H_3COO)_3$	12+
NH_4VO_3	3+

3. Red phosphors

Activator used for red phosphor is Eu^{3+} ($4f^6$) and the commonly used hosts are Y_2O_3, Gd_2O_3, YVO_4 and $LnBO_3$, Ln = La, Gd and Y.

3.1. Combustion synthesis of Eu^{3+} activated oxide red phosphors [57]

For the combustion synthesis of these phosphors, the appropriate metal nitrate, europium nitrate and fuel, either ODH or urea were used. When ODH was used as the fuel, the combustion was flaming and the flame temperature measured using optical pyrometer was about 1400 °C ± 100 °C. But, combustion behaviour was smouldering (without flame) when urea was employed in the combustion process. Theoretical equation assuming complete combustion may be written for Eu^{3+} activated Y_2O_3 red phosphor using ODH as the fuel as follows.

$$2 - xY(NO_3)_3 + xEu(NO_3)_3 + 3C_2H_6N_4O_2(\text{ODH}) \rightarrow \underset{\text{(red phosphor)}}{Y_{2-x}Eu_xO_3(s)} + \text{by products}$$

where $x = 0.05$.

Fig. 1 shows powder XRD of Eu^{3+} doped Y_2O_3 red phosphor synthesized by ODH and urea methods. It is clear that ODH process shows very sharp powder XRD pattern and urea process exhibits very broad powder XRD peaks. Therefore, by changing the fuel one can control particulate properties (Specific surface areas = 22 and 13 m^2/g for urea and ODH processes).

3.2. Combustion synthesis of Eu^{3+} activated borate and vanadate red phosphors [58]

For the combustion synthesis of borate red phosphors, aqueous solution of $Ln(NO_3)_3$, H_3BO_3 and ODH was heated at 400 °C in air. Boric acid is a neutral compound and hence, neither extra ammonium nitrate nor fuel was required. Whereas, ammonium meta vanadate was used as source for vanadium in the vanadate red phosphor preparation. Therefore, ammonium meta vanadate served as reducer and hence, completely decomposable ammonium nitrate was used as oxidizer. Formation of borate and vanadate by combustion may be represented by the following reactions.

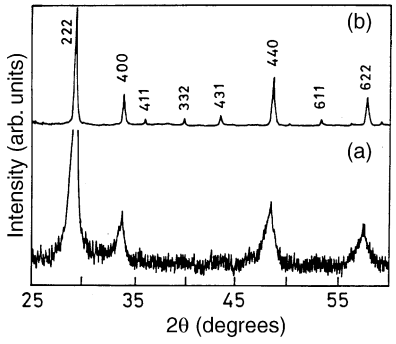

Fig. 1. Powder XRD patterns of combustion synthesized Y_2O_3:Eu^{3+} (a) urea process, and (b) ODH process.

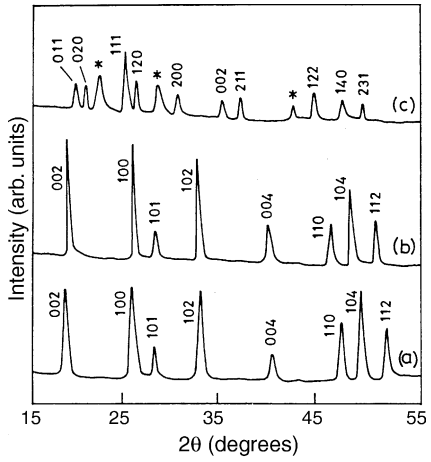

Fig. 2. Powder XRD patterns of combustion prepared $LnBO_3$ (ODH process) (a) Ln = Y, (b) Ln = La and (c) Ln = Gd, where * monoclinic $GdBO_3$.

$$2Ln(NO_3)_3 + \underset{\text{(ODH)}}{3C_2H_6N_4O_2} \rightarrow Ln_2O_3(s) + \text{by product}$$

$$4Ln(NO_3)_3 + \underset{\text{(3MP5O)}}{3C_4H_6N_2O} \rightarrow 2Ln_2O_3(s) + \text{by product}$$

$$2H_3BO_3 \rightarrow B_2O_3(s) + 3H_2O(g)$$

$$2NH_4VO_3 + 3NH_4NO_3 \rightarrow V_2O_5(s) + \text{by product}$$

The products formed Ln_2O_3, B_2O_3, V_2O_5 further react to give corresponding metal borates and metal vanadate. Fig. 2 shows the powder XRD patterns of as-prepared $LnBO_3$ (Ln = La, Gd and Y) (ODH fuel). It reveals that except for $GdBO_3$, other borates are single phase crystalline compounds. Thermal evolution of $GdBO_3$ was carried out using powder XRD. Fig. 3 shows the powder XRD patterns of as-prepared and calcined $GdBO_3$. It indicates that single phase $GdBO_3$ could be obtained by calcining it at 900 °C for 1 h. As-formed YVO_4 (3-methyl-pyrazole-5-one, $C_4H_6N_2O$3MP5O process) was X-ray amorphous which on heating at 650 °C for 1 h showed crystalline phase (Fig. 4). The amorphous yttrium vanadate could be crystallized to single phase material at 650 °C compared to >1000 °C required in the ceramic method [59]. The low calcinations temperature required to form the desired phase may be attributed to the formation of fine and reactive Y_2O_3 and V_2O_5 powders in the combustion process.

3.3. Precursor method for the synthesis of oxide red phosphor

Eu^{3+} activated red phosphor was also synthesized from redox compound/fuel rich compound or in other words, valency of the compound is positive and hence, it is

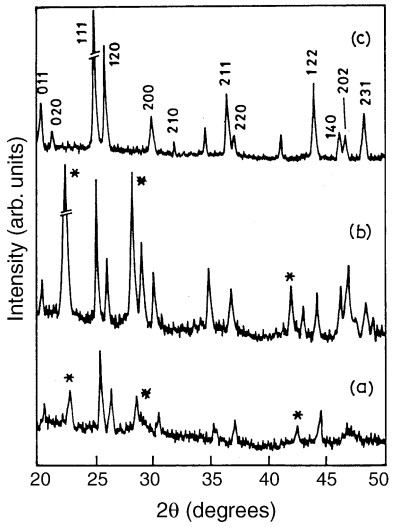

Fig. 3. Powder XRD patterns of $GdBO_3$:Eu^{3+} (a) as-prepared, (b) 700 °C, and (c) 900 °C, where * monoclinic $GdBO_3$.

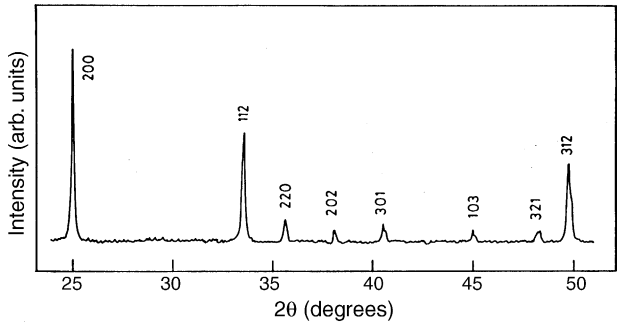

Fig. 4. Powder XRD of heat treated at 650 °C YVO_4:Eu^{3+} red phosphor (3MP5O process).

called fuel containing Eu^{3+} and Y^{3+}. Eu^{3+} and Y^{3+} form the following compounds with hydrazine carboxylate ligand ($N_2H_3COON_2H_5$), $Y(N_2H_3COO)_3{\cdot}3H_2O$ and $Eu(N_2H_3COO)_3{\cdot}3H_2O$. Powder XRD patterns (Fig. 5) of

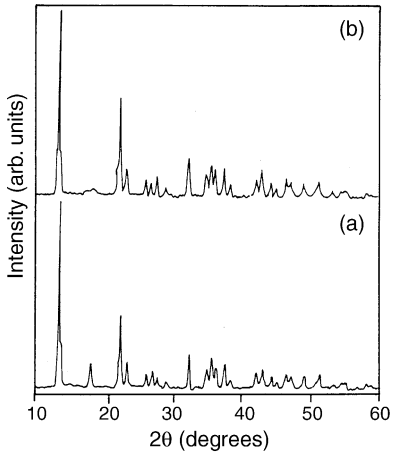

Fig. 5. Powder XRD patterns of $Y(N_2H_3COO)_3{\cdot}3H_2O$ and $Eu(N_2H_3COO)_3{\cdot}3H_2O$.

these complexes are very similar to each other and hence, these complexes form solid solution when treated Eu^{3+} and Y^{3+} salts with hydrazine carboxylates. Thus, Yttrium (III) chloride and europium (III) chloride were treated with hydrazine carboxylate, $N_2H_3COON_2H_5$ at room temperature. This reaction yields yttrium europium hydrazine carboxylate precursor, $(Y_{0.975}Eu_{0.025})(N_2H_3COO)_3{\cdot}3H_2O$. This compound was decomposed in air in the temperature range 600–1000 °C to get red phosphor. Or the redox compound was mixed with calculated amount of either ammonium nitrate or ammonium perchlorate and was rapidly heated at 300 °C to get Eu^{3+} doped red phosphor [60].

3.4. Luminescent properties of red phosphors

3.4.1. Eu^{3+} activated oxide red phosphors

Y_2O_3 has two different crystallographic sites (C_2 and S_6) for Y^{3+} ion [61]. C_2 and S_6 sites are present in 3:1 ratio. Therefore, Eu^{3+} has equal probability of occupying C_2 and S_6 site. Eu^{3+} occupying C_2 site shows characteristic red-orange emission (Fig. 6) at 611 nm. This emission at 611 nm is due to electric dipole transition. It is very sharp and looks like atomic emission. This characteristic emission band is attributed to the electric dipole transition, $^5D_0 \rightarrow {}^7F_2$ of the Eu^{3+} ions [62]. Other transitions of Eu^{3+} are also seen in the fluorescent spectra but these are very weak. This is usually observed if the product is homogeneous, which

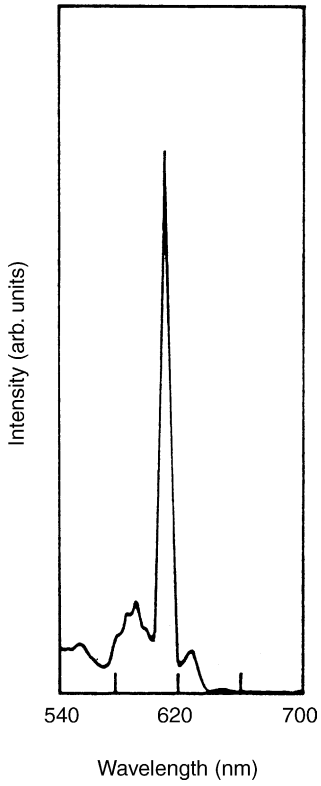

Fig. 6. Emission spectrum of $Y_{1.95}Eu_{0.05}O_3$ (ODH process). Excitation wave length was 254 nm.

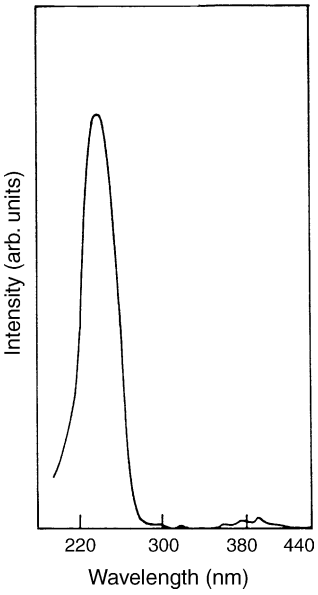

Fig. 7. Excitation spectrum of $Y_{1.95}Eu_{0.05}O_3$ (ODH process) when the emission wave length was 611 nm.

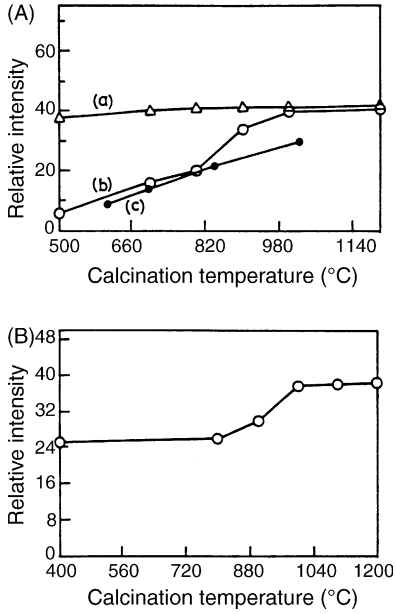

Fig. 8. (A) Effect of calcination on luminescence of Y_2O_3:Eu^{3+} Gd_2O_3:Eu^{3+} red phosphors. (a) ODH process, (b) urea process, and (c) from hydrazine carboxylate complex. (B) Gd_2O_3:Eu^{3+} (ODH process).

favour strong energy transfer from S_6 to C_2 [11]. Fig. 7 shows excitation spectrum of Y_2O_3:Eu^{3+}. It shows very broad beak and this peak falls in the region of 254 nm. This excitation peak is due to charge transfer from oxygen to europium (III) ion. Similarly, Eu^{3+} activated Gd_2O_3 was also prepared by solution combustion method using gadolinum nitrate, europium nitrate and oxalyl dihydrazide/urea. Fluorescent spectrum of Gd_2O_3:Eu^{3+} was very similar to that of Y_2O_3:Eu^{3+}.

3.4.2. Effect of calcinations on luminescence of Eu^{3+} red phosphors

Combustion synthesized red phosphors (ODH process, urea process and precursor method) were calcined at different temperature in order to know the effect of calcinations on their luminescent properties. Calcination does not affect the position of emission wavelengths of all combustion synthesized red phosphors. It indicates that Eu^{3+} environment is not affected by calcinations. Fig. 8 illustrates the effect of calcinations on emission intensity (611 nm) of Y_2O_3:Eu^{3+} and Gd_2O_3:Eu^{3+} red phosphors. For all the fluorescent experiments, the excitation wave length was kept as 254 nm. Y_2O_3:Eu^{3+} (ODH process) phosphor shows a slight increase in emission intensity whereas Y_2O_3:Eu^{3+} (urea process and precursor process) and Gd_2O_3:Eu^{3+} (ODH process) red phosphors exhibit remarkable increase in emission intensity. The increase in emission intensity is observed in the temperature range 500–800 °C. But, beyond 1000 °C, calcination does not alter the emission intensity significantly. The increase in emission intensity of the combustion synthesized these red phosphors on calcinations may be attributed to improved crystalline.

3.4.3. Effect of impurity ions on luminescence of Eu^{3+} activated red phosphors

Impurity ions such as Ca^{2+}, Mg^{2+}, Zn^{2+}, Ce^{4+}, Zr^{4+}, Gd^{3+} (∼2.5 mol%) were doped in Y_2O_3:Eu^{3+} to study their influence on the luminescence of Eu^{3+}. The position of emission wavelengths of Y_2O_3:Eu^{3+} is not affected by the addition of impurity ions. But, the emission intensity is influenced by the addition of the impurity ions. This indicates that environment around Eu^{3+} is not influenced by the addition of impurity ions. Table 2 summarizes relative emission intensity of Eu^{3+} with different impurity ions. Addition of divalent metal ions enhances the emission intensity, whereas tetravalent metal ions decrease the emission intensity. However, trivalent metal ions do not alter the emission intensity significantly.

Since doping of calcia shows appreciable effect, detailed studies on calcia doped Y_2O_3:Eu^{3+} were carried out. Fig. 9 shows the fluorescence spectra of calcia doped and undoped Y_2O_3:Eu^{3+} red phosphors. Calcia doped Y_2O_3:Eu^{3+} shows 10-fold increase in emission intensity. The enhanced emission intensity of Eu^{3+} by the addition of Ca^{2+} may be attributed to reduction of interstitial oxygen [63] (interstitial

Table 2
Effect of impurity ions on luminescence of Eu^{3+}

Phosphor, $Y_{1.90}M_{0.05}Eu_{0.05}O_3$	Relative emission intensity of 611 nm
–	35
Ca^{2+}	450
Mg^{2+}	420
Zn^{2+}	385
Gd^{3+}	31
La^{3+}	33
Ce^{4+}	26
Zr^{4+}	28

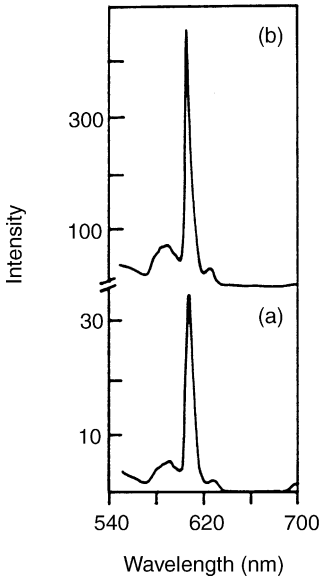

Fig. 9. Fluorescence spectra of CaO doped and undoped $Y_{2-x}Ca_xO_3:Eu^{3+}$ red phosphor (a) $x = 0$ and (b) $x = 0.05$. $\lambda_{exc} = 254$ nm.

oxygen absorbs part of the excitation radiation and exhibits no emission). Calcia content was increased in the formula, $Y_{1.95-x}Ca_xEu_{0.05}O_3$ in order to investigate its effect on the luminescent properties of Eu^{3+}. Typical powder XRD patterns of as prepared $Y_{1.95-x}Ca_xEu_{0.05}O_3$ phosphors ($x = 0.5$ and $x = 0.75$) are shown in Fig. 10. It can be seen that up to $x = 0.5$, formation of single phase is observed. For $x = 0.75$, presence of CaO is also observed. Fig. 11 shows the plot of calcium content versus relative emission intensity. It reveals that emission intensity is more at the initial calcia addition. Further addition of calcia increases the relative emission intensity slightly up to $x = 0.5$. Beyond the value of $x = 0.5$, drop in emission intensity is seen in the plot. The decrease in emission intensity may be attributed to the formation of non-luminescent calcia or less luminescence of Eu^{3+} doped CaO. The presence of calcia was confirmed by the powder XRD pattern of as-prepared phosphor (Fig. 10). Thus, expensive yttrium could be substituted by inexpensive calcium upto 25 mol% without affecting the luminescence of Eu^{3+}.

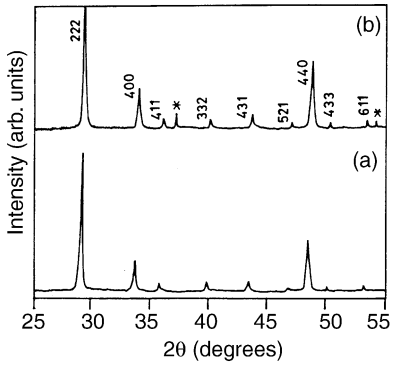

Fig. 10. Powder XRD patterns of as-prepared $Y_{1.95-x}Ca_xEu_{0.05}O_3$ red phosphors (a) $x = 0.5$ and (b) $x = 0.75$ where * indicates CaO.

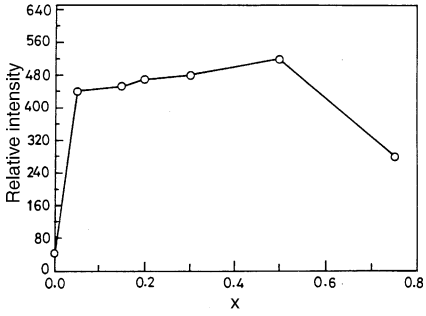

Fig. 11. Plot of calcium content and emission intensity of $Y_{1.95-x}Ca_xEu_{0.05}O_3$ red phosphor.

3.4.4. Luminescent properties of Eu^{3+} activated borate red phosphors

The borates of the lighter rare earths (lanthanum to neodymium) possess the aragonite structure: orthorhombic with Pnam as the space group [64]. The lanthanum, occupying the 4c crystallographic position, has a Cs point site symmetry. The borates of the heavier rare earths (samarium to luetetium) have the vaterite structure with an octahedrally coordinated and 12-coordinated sites for Ln^{3+} ions in the ratio 2:1, respectively. For the 12-coordinated site, six oxygen neighbours are at shorter distances while the other six oxygens are at longer distances. Eu^{3+} occupies at the rare-earth ion site and exhibits different luminescent properties.

Fig. 12 shows the fluorescence spectra of Eu^{3+} doped $LnBO_3$ (Ln = La, Gd and Y). It shows characteristic red orange emission. The emission spectrum of $LaBO_3:Eu^{3+}$ consists of two bands at 615 and 595 nm and these bands are attributed to $^5D_0 \rightarrow {}^7F_2$ and $^5D_0 \rightarrow {}^7F_1$ transition of 9-coordinated Eu^{3+} ions, respectively. But, there are three bands at 625, 610 and 595 nm observed for $GdBO_3:Eu^{3+}$ and $YBO_3:Eu^{3+}$ phosphors. The band at 595 nm is attributed to magnetic dipole $^5D_0 \rightarrow {}^7F_1$ transition of Eu^{3+}, whereas the bands at 625 nm and 610 nm are attributed to electric dipole $^5D_0 \rightarrow {}^7F_2$ transition for 12 and 8 coordinated Eu^{3+} ions, respectively. Since electric dipole transition, $^5D_0 \rightarrow {}^7F_2$ depends upon the structure, there are two bands observed for different coordinated Eu^{3+} in $GdBO_3:Eu^{3+}$ and $YBO_3:Eu^{3+}$.

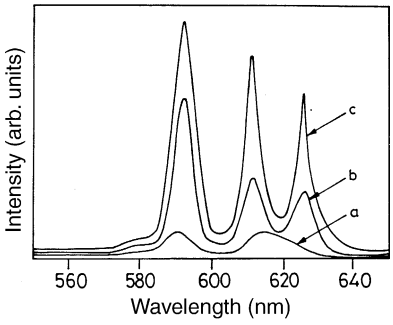

Fig. 12. Fluorescence spectra of Eu^{3+} activated $LnBO_3:Eu^{3+}$ red phosphor (a) Ln = La; (b) Ln = Gd and (c) Ln = Y. Excitation wave length was 254 nm.

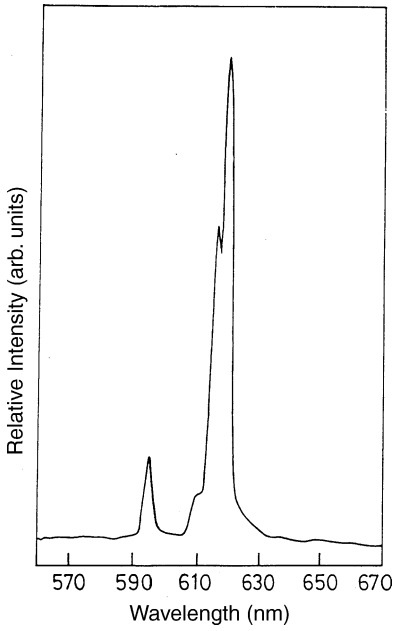

Fig. 13. Fluorescence spectra of Eu^{3+} activated YVO_4 red phosphor (3MP5O process). Excitation wave length was 254 nm.

3.4.5. *Luminescent properties of Eu^{3+} activated vanadate red phosphors*

Yttrium vanadate is a tetragonal crystal structure having the $ZrSiO_4$ structure and the space group is I41/amd [65]. In this structure the vanadium atoms are tetrahedrally coordinated with oxygen atoms, while yttrium ions are surrounded by eight oxygen neighbours arranged in the form of two distorted tetrahedral. Eu^{3+} occupies at eight-coordinated Y^{3+} site in YVO_4.

Fluorescence spectrum of $Y_{0.95}Eu_{0.05}VO_4$ is shown in Fig. 13. It shows emissions at 595, 611, 615 and 619 nm. The bands at 611, 615 and 619 nm result from $^5D_0 \geq {}^7F_2$ transition for Eu^{3+} ion. The crystal field splitting of the $^7F_2$ level can lead to five distinguishable states, and the transition at 611, 615 and 619 nm differ in regard to the particular $^7F_2$ state on which they terminate [53]. The emission at 595 nm is due to $^5D_0 \geq {}^7F_1$ transition as reported. Fig. 14 shows the plot of relative emission intensity of YVO_4:Eu^{3+} as a function of calcinations temperature. Emission intensity of YVO_4:Eu^{3+} (619 nm) increases in the temperature range 400–600 °C. Then, it increases moderately up to 1000 °C and remains almost unaffected beyond 1000 °C. Improved crystallanity may be responsible for the increase in the emission intensity with calcinations temperature.

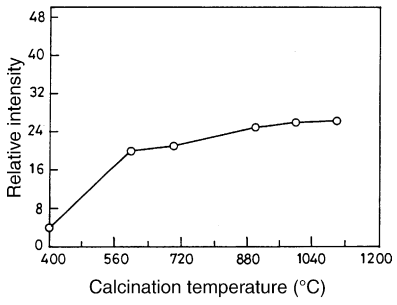

Fig. 14. Plot of relative emission intensity of YVO_4:Eu^{3+} as a function of calcinations temperature.

3.5. *Blue phosphors [66]*

The activator used for blue phosphor is Eu^{2+} and the commonly used hosts are $BaMgAl_{10}O_{17}$, $BaMg_2Al_{16}O_{27}$ and $Ba_{0.64}Al_{12}O_{18.64}$.

3.5.1. *Combustion synthesis of Eu^{2+} activated blue phosphors*

Eu^{2+} doped barium based compounds were prepared by rapidly heating an aqueous concentrated solution containing stoichiometric amounts of metal nitrates and a fuel (carbohydrazide or diformyl hydrazine or urea) at 400/500 °C. Theoretical equation for the formation of $BaMgAl_{10}O_{17}$:Eu^{2+} and $0.64BaO{\cdot}6Al_2O_3$:Eu^{2+} from $M(NO_3)_2$ (M = Ba and Mg), $M(NO_3)_3$ (M = Al and Eu) and urea at 500 °C, assuming complete combustion, may be written as

$$0.64 - x\mathrm{Ba(NO_3)_2} + x\mathrm{Eu(NO_3)_3} + 12\mathrm{Al(NO_3)_3} + 23.3\mathrm{CH_6N_4O(CH)} \rightarrow \underset{\text{(blue phosphor)}}{\mathrm{Ba_{0.64-}}_x\mathrm{Eu}_x\mathrm{Al_{12}O_{18.64}}(s)} + \text{by product}$$

$$1 - x\mathrm{Ba(NO_3)_2} + x\mathrm{Eu(NO_3)_3} + \mathrm{Mg(NO_3)_2} + 10\mathrm{Al(NO_3)_3} + 28.33\mathrm{CH_4N_2O(urea)} \rightarrow \underset{\text{(blue phosphor)}}{\mathrm{Ba}_{1-x}\mathrm{Eu}_x\mathrm{MgAl_{10}O_{17}}(s)} + \text{by products}$$

Formation of blue phosphors was confirmed by powder XRD. Fig. 15 shows the powder XRD patterns of Eu^{2+} doped

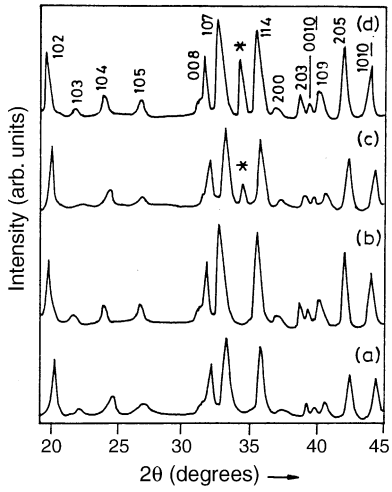

Fig. 15. Powder XRD patterns of Eu^{2+} doped $x{\cdot}BaO{\cdot}6Al_2O_3$, (a) $x = 0.64$; (b) $x = 0.82$; (c) $x = 1.00$ and (d) $x = 1.3$, where * $BaAl_2O_4$.

xBaO.6Al_2O_3, x = 0.64–1.3. It is observed that hexa aluminate having barium content lower than 0.82 does not show any additional XRD. When $x > 0.82$, additional peaks corresponding to those of $BaAl_2O_4$ are noticed. Quantity of $BaAl_2O_4$ increases with increase of the barium content in barium hexa aluminate. According to Kimura and coworkers [67], coexistence of two phases (barium poor and barium rich) was indicated by the splitting in (1 0 7) reflections, whereas according to Smets et al. [68] splittings of (0 0 1) reflections are more diagnostic indicators of the phase multiplicity. Therefore, selected reflections were recorded under slow scanning mode for high resolution. No splitting was observed in any one of these reflections for the as-prepared as well as calcined (1300 °C) phosphor. These results indicate that the phosphors obtained by the combustion process are monophasic nonstoichiometric hexa aluminate.

3.5.2. Luminescent properties of Eu^{2+} activator blue phosphors

Both $BaMgAl_{10}O_{17}$ and $BaAl_{12}O_{19}$ are structurally related to hexagonal beta-alumina, $NaAl_{11}O_{17}$ [69,70]. Beta-alumina is built out of spinel blocks separated by an intermediate layer, which accommodates two large ions Na^+ and O^{2-} per spinel blocks. In this structure when all Na^+ ions are replaced by Ba^{2+} and Al^{3+} ions are replaced by Mg^{2+} in the spinel blocks maintaining charge balance to obtain $BaMgAl_{10}O_{17}$. But, to get $BaAl_{12}O_{19}$ 75% of the sodium ions are randomly replaced by Ba^{2+} and 25% by O^{2-} in beta-alumina $NaAl_{11}O_{17}$. Eu^{2+} occupies at barium site to exhibit blue emission.

Presence of Eu^{2+} was confirmed by fluorescence spectra. Emission spectra of as-prepared Eu^{2+} activated $BaMgAl_{10}O_{17}$, $BaMg_2Al_{16}O_{27}$ and $Ba_{0.64}Al_{12}O_{18.64}$ show characteristic blue emission at 450, 450 and 435 nm, respectively (Fig. 16). The concentration of Eu^{2+} in $BaMgAl_{10}O_{17}$ was optimised in order to obtain maximum UV stability with minimum concentration quenching. The phosphors with activator concentration ranging from 2 to 20 mol% were prepared by the combustion of corresponding metal nitrates and urea at 500 °C. The as-prepared phosphors showed single phase crystalline nature. The room temperature fluorescence spectra of all the phosphors were recorded under the same condition by exciting at 254 nm and the relative emission intensity was monitored. It revealed that relative emission intensity increased with increasing activator concentration. Above the 16 mol% activator concentration, sudden drop in relative emission intensity was observed and it is probably due to concentration quenching. Hence, 16 mol% was found to be the optimum concentration of activator for maximum emission intensity.

Fig. 17 shows emission spectra of Eu^{2+} doped xBaO.6Al_2O_3 ($0.64 < x > 1.3$). All the phosphors show characteristic emission in blue region (435–462 nm). This emission band is attributed to Eu^{2+} $4f^6 5d \rightarrow 4f^7$ transition. It is noticed that with increase in barium content the emission band shifts towards longer wavelength. The shift in emission band towards longer wavelength at higher barium concentration may be attributed to formation of Eu^{2+} doped $BaAl_2O_4$. It has been reported that Eu^{2+} doped barium aluminate ($BaAl_2O_4$) shows emission band at 505 nm [71]. This observation is confirmed by the powder XRD (Fig. 15), which shows the presence of $BaAl_2O_4$ in the barium rich compositions. Since solution combustion process involve atomic level homogeneity of starting materials, doping of Eu^{2+} takes place at barium site in both barium hexa aluminate and barium aluminate spinel.

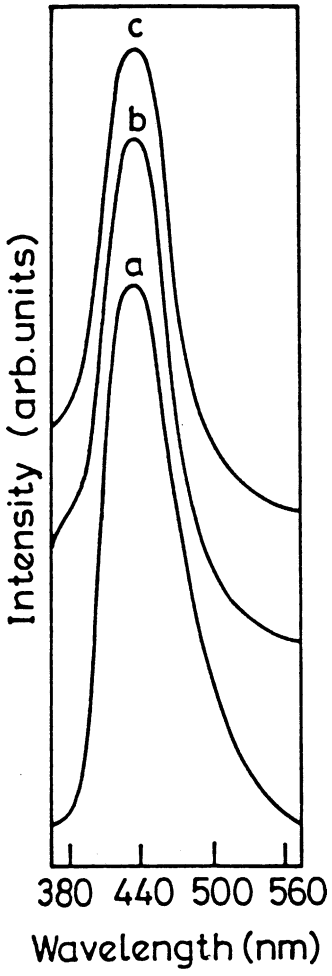

Fig. 16. Emisssion spectra of Eu^{2+} activated (a) $BaMgAl_{10}O_{17}$, (b) $BaMg_2Al_{16}O_{27}$ and (c) $Ba_{0.64}Al_{12}O_{18.64}$ blue phosphors (urea process). Excitation wave length was 254 nm.

3.6. Green phosphors [72]

Tb^{3+} is commonly used as activator for the green emission. The oxide host employed for Tb^{3+} green emission is (La,Ce)$MgAl_{11}O_{19}$. Other possible green phosphors for fluorescent lamps are (Ce,Gd)MgB_5O_{10}:Tb^{3+} and (La,Ce)PO_4:Tb^{3+}.

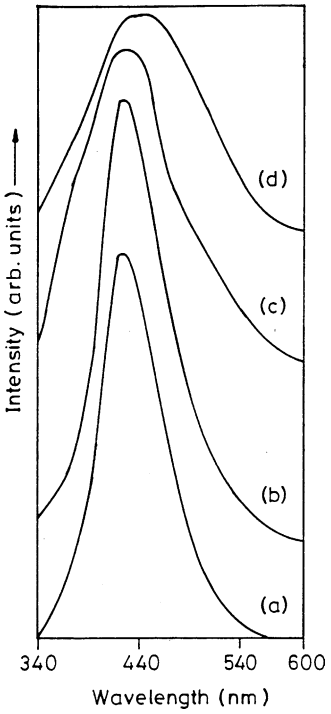

Fig. 17. Emission spectra of Eu^{2+} doped xBaO.6Al_2O_3 (a) $x = 0.64$; (b) $x = 0.82$; (c) $x = 1.0$ and (d) $x = 1.3$. Excitation wave length was 254 nm.

3.6.1. Combustion synthesis of Tb^{3+} activated green phosphor

Tb^{3+} activated (La,Ce)$MgAl_{11}O_{19}$ green phosphor was obtained by rapidly heating an aqueous concentrated solution containing stoichiometric amounts of metal nitrates ($La(NO_3)_3$, $Ce(NO_3)_3$, $Tb(NO_3)_3$, $Mg(NO_3)_2$) and urea/diformyl hydrazine redox mixture at 500 °C. The stoichiometric composition of the redox mixtures for the combustion was calculated using the total oxidizing (O) and reducing (F) valencies. Thus, $M(NO_3)_2$:urea (1:1.66), $M(NO_3)_3$:urea (1:2.5), $M(NO_3)_2$:DFH (1:1.25) and $M(NO_3)_3$:DFH (1:1.88) redox compositions were used for combustion. Theoretical equation assuming complete combustion can be written as follows.

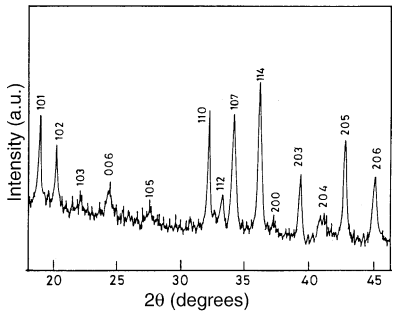

Fig. 18. Powder XRD pattern of $(La_{0.15}Ce_{0.5}Tb_{0.35})MgAl_{11}O_{19}$ (urea process).

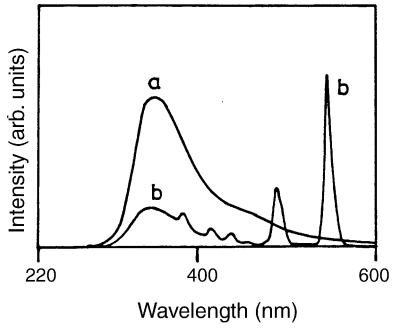

Fig. 19. Emission spectrum of (a) $(La_{0.98}Ce_{0.02})MgAl_{11}O_{19}$, (b) $(La_{0.98}Ce_{0.02})MgAl_{11}O_{19}:Tb^{3+}$. Excitation wave length was 254 nm.

$$1 - x\mathrm{Ce(NO_3)_3} + x\mathrm{Tb(NO_3)_3} + \mathrm{Mg(NO_3)_2} + 11\mathrm{Al(NO_3)_3} + 31.67\mathrm{CH_4N_2O(urea)} \rightarrow \underset{\text{(green phosphor)}}{\mathrm{Ce_{1-x}Tb_xMgAl_{11}O_{19}}(s)} + \text{by product}$$

Fig. 18 shows the powder XRD pattern of $LaMgAl_{11}O_{19}$, which reveals single phase crystalline nature. This observation is notable because conventional ceramic synthesis of $LaMgAl_{11}O_{19}$ requires elevated temperature (>1400 °C) and always contains Al_2O_3 as impurity [59].

3.6.2. Luminescent properties of Tb^{3+} activated green phosphors

$LaMgAl_{11}O_{19}$ is having a true magnetoplumbite-like structure similar to hexagonal rare-earth aluminates [73]. This structure is related to the structure of the betal-aluminas. It consists of spinel blocks separated by an intermediate layer containing three oxygen, one rare-earth, and one aluminium ion per spinel blocks. The Mg^{2+} ions are accommodated into the spinel blocks as in $BaMgAl_{10}O_{17}$.

Emission spectrum of combustion synthesized $(La_{0.98}Ce_{0.02})MgAl_{11}O_{19}$ shows a broad band at 340 nm (Fig. 19a). The emission of Ce^{3+} is due to $4f^6 5d \rightarrow {}^2F_j$ (with j = 5/2 and 7/2) transition. Addition of Tb^{3+} in $(La_{0.98}Ce_{0.02})MgAl_{11}O_{19}$ resulted in emissions at 480 and 543 nm in addition to Ce^{3+} emission (Fig. 19b). The Tb^{3+} emissions, which arise due to energy transfer from Ce^{3+}, are attributed to ${}^5D_3 \rightarrow {}^7F_5$ and ${}^5D_4 \rightarrow {}^7F_5$ transitions. In order to minimize the ultraviolet Ce^{3+} emission (340 nm), Tb^{3+} concentration was increased in the formula, $(La_{0.98-x}Tb_xCe_{0.02})MgAl_{11}O_{19}$. Fig. 20 illustrates the effect of terbium concentration on the luminescence of Ce^{3+} and Tb^{3+} in $LaMgAl_{11}O_{19}$ when the excitation wavelength was 254 nm. With the increase in Tb^{3+} concentration, emission intensity of Tb^{3+} increases at the expense of Ce^{3+} emission intensity. This observation may be attributed to increased availability of Tb^{3+} for absorbing the Ce^{3+} emission. The Tb^{3+} emission intensity increases up to $x = 0.35$ and beyond the value of $x = 0.35$, there is a drop in emission intensity of Tb^{3+}. But, ultraviolet Ce^{3+} emission continues to decrease with increasing Tb^{3+} concentration.

Table 3
Luminescent properties of $LaMgAl_{11}O_{19}:Ce^{3+},Tb^{3+},Eu^{2+}$

Phosphors	Emission wavelength[#], nm		
	Eu^{2+}	Ce^{3+}	Tb^{3+}
$LaMgAl_{11}O_{19}:Ce^{3+}$ (10)	–	349(738)	–
$LaMgAl_{11}O_{19}:Eu^{2+}$ (5)	442(714)		
$LaMgAl_{11}O_{19}:Ce^{3+}$ (10), Eu^{2+} (5)	442(1277)	351(320)	–
$LaMgAl_{11}O_{19}:Tb^{3+}$ (8), Eu^{2+} (5)	441(310)	–	542(202)
$LaMgAl_{11}O_{19}:Ce^{3+}$ (10), Tb^{3+} (8), Eu^{2+} (5)	437(615)	354(68)	542(457)

[#] Excitation wavelength = 254 nm; Parentheses = Intensity.

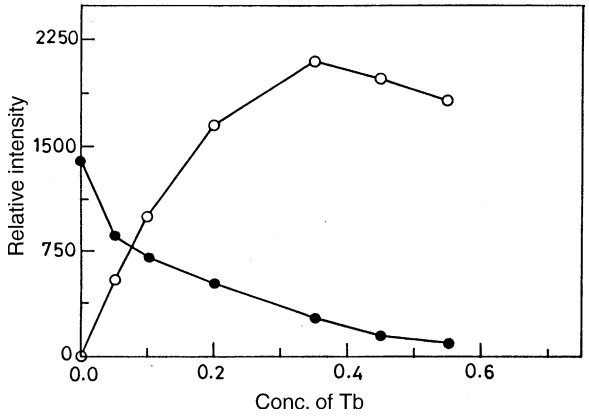

Fig. 20. Plot of emission intensities of Ce^{3+} and Tb^{3+} with concentration of Tb^{3+} in $(La_{0.98-x}Tb_xCe_{0.02})MgAl_{11}O_{19}$ green phosphors. (○) Tb^{3+} emission, (●) Ce^{3+} emission.

The decrease in emission intensity of Tb^{3+} ($x > 0.35$) may be attributed to concentration quenching. Fig. 21 shows the plot of cerium concentration versus emission intensities of Ce^{3+} and Tb^{3+} in $(La_{0.63-x}Tb_{0.35}Ce_x)MgAl_{11}O_{19}$. It reveals that with increase in Ce^{3+} concentration, Tb^{3+} emission also increases, whereas Ce^{3+} emission intensity decreases. For the value of $x > 0.3$, emission intensity of Tb^{3+} remains unchanged. But, emission intensity of Ce^{3+} decreases. Therefore, maximum Tb^{3+} emission is observed for $(La_{0.15}Ce_{0.5}Tb_{0.35})MgAl_{11}O_{19}$ green phosphor. Substitution of La^{3+} by Gd^{3+} in the green phosphor does not affect the luminescence of Tb^{3+}. But, substitution of La^{3+} by Sm^{3+} quenched Tb^{3+} emission.

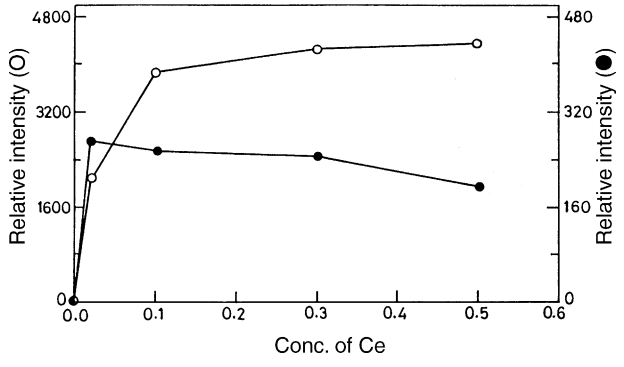

Fig. 21. Plot of emission intensities of Ce^{3+} and Tb^{3+} with concentration of Ce^{3+} in $(La_{0.63-x}Ce_xTb_{0.35})MgAl_{11}O_{19}$ green phosphor.

Since $LaMgAl_{11}O_{19}$ can also be a host for Eu^{2+}, investigations were carried out to study the effect of simultaneous doping of Ce^{3+}, Tb^{3+} and Eu^{2+} in $LaMgAl_{11}O_{19}$. The luminescence properties of these ions are summarized in Table 3. The results indicate that the addition of Ce^{3+} enhances Eu^{2+} emission with a decrease in emission intensity of Ce^{3+}. Where as the addition of Tb^{3+} decreases the Eu^{2+} emission intensity. Hence, Eu^{2+} can also be used as a sensitizer for Tb^{3+}. Unlike Ce^{3+}, Eu^{2+} sensitizer does not emit in the ultraviolet region. However, Tb^{3+} emission intensity is greater when Ce^{3+} is used as a sensitizer. The increase in the Eu^{2+} emission may be due to non-radiative energy transfer from Ce^{3+} to Eu^{2+}. Co-doping of all the activators resulted in emission at 437 (Eu^{2+}), 354 (Ce^{3+}), and 490 and 542 nm (Tb^{3+}).

4. Conclusions

Rare earth doped lamp phosphors obtained by versatile solution combustion process are single phase in nature except $Gd_2O_3:Eu^{3+}$, $GdBO_3:Eu^{3+}$ and $YVO_4:Eu^{3+}$. The formation of homogeneous single phase lamp phosphors not only demonstrates the capability of the combustion process in the atomic level doping of impurity ions in the host lattices but also confirms the highly exothermic nature of combustion. The major advantages of the combustion process are improvement in processing time, energy saving and the fine particle nature of the combustion products.

References

[1] G. Blasse, B.C. Grabmair, Luminescent Materials, Springer Verlag, Berlin, 1994.
[2] T. Welker, J. Lumin. 48/49 (1991) 49.
[3] G. Blasse, J. Alloys Compd. 192 (1993) 17.
[4] Proceedings of the 2nd International Conference on f-element, J. Alloys Compd., 1995, pp. 225.
[5] The First International Conference on the Science and Technology of Emissive Displays and Lighting, 12–14 November 2001, San Diego, CA, USA.
[6] Phosphor Global Summit, Scottsdale, AZ, USA, 19–21 March 2003.
[7] Phosphor Global Summit, Marriott Biscane Bay, Miami, FL, USA, 16–18 March 2004.
[8] Proceedings of the International Conference Rare earths' 92, J. Alloys Compd., Kyoto, 1993, pp. 192.

[9] F. Laville, D. Gourier, A.M. Lejus, D. Vivien, J. Solid State Chem. 49 (1983) 180.
[10] K.A. Wickersheim, R.A. Lefever, J. Electrochem. Soc. 111 (1964) 47.
[11] R.C. Ropp, J. Electrochem. Soc. 111 (1964) 311.
[12] N.C. Chang, J. Appl. Phys. 34 (1963) 3500.
[13] R.B. Hunt Jr., R.G. Pappalardo, J. Lumin. 34 (1985) 133.
[14] P. Maestro, D. Huguenin, A. Seigneurin, P. Deneuve, P. Le Lann, J.F. Berar, J. Electrochem. Soc. 139 (1992) 1479.
[15] M. Buijs, A. Meijerink, G. Blasse, J. Lumin. 37 (1987) 9.
[16] D.B.M. Klaasen, R.A.M. van Ham, T.G.M. van Rijn, J. Lumin. 43 (1989) 261.
[17] R.G. Pappalardo, R.B. Hunt Jr., J. Electrochem. Soc. 132 (1985) 721.
[18] L.H. Brixner, E. Abramson, J. Electrochem. Soc. 112 (1965) 70.
[19] F. Laville, M. Perrin, A.M. Lejus, M. Gasperin, R. Moncorge, D. Vivien, J. Solid State Chem. 65 (1986) 301.
[20] H.T. Hintzen, H.M. van Noort, J. Phys. Chem. Solids 49 (1988) 873.
[21] F.C. Palilla, A.K. Levine, M. Rinkevics, J. Electrochem. Soc. 112 (1965) 776.
[22] E. Antic-Fidancev, M. Lemaitre-Blaise, J. Chaminade, P. Porcher, J. Alloys Compd. 180 (1992) 223.
[23] J. Systma, A. Meijer, G. Blasse, J. Solid State Chem. 99 (1992) 78.
[24] G. Blasse, A. Bril, Philips Tech. Rev. 31 (1970) 303.
[25] G. Blasse, Chem. Mater. 1 (1989) 294.
[26] B.M.J. Smets, Mater. Chem. Phys. 16 (1987) 283.
[27] G. Blasse, Chem. Mater. 6 (1994) 1465.
[28] S.L. Issler, C.C. Torardi, J. Alloys Compd. 229 (1995) 54.
[29] C.R. Ronda, J. Alloys Compd. 225 (1995) 534.
[30] G. Blasse, J. Alloys Compd. 225 (1995) 529.
[31] P. Maestro, D. Huguenin, J. Alloys Compd. 225 (1995) 520.
[32] E. Banks, J. Electrochem. Soc. 125 (1978) 415C.
[33] C.R. Ronda, T. Justel, H. Nikol, J. Alloys Compd. 275–277 (1998) 669.
[34] T. Justel, H. Nikol, C. Ronda, Angew. Chem. Int. Ed. 37 (1998) 3084.
[35] R.C. Ropp, Luminescence and the Solid State, Elsevier Science, Amsterdam, 1991.
[36] P. Wacher, D.J. Bracco, F.C. Palilla, Electrochem. Technol. 5 (1967) 358.
[37] R.E. Newnham, M.J. Redman, R.P. Santoro, J. Am. Chem. Soc. 46 (1963) 253.
[38] J.M.P.J. Verstegen, J.L. Sommerdijk, J.G. Verriet, J. Lumin. 6 (1973) 425.
[39] A.G. Avanesov, K.B. Achmiz, P.I. Bykovskii, Yu.A. Kuzenetsov, V.F. Pisarenko, N.G. Chernaya, Inorg. Mater. 17 (1981) 579.
[40] B.M.J. Smets, J.G. Verlijsdonk, Mater. Res. Bull. 21 (1986) 1305.
[41] J.M.P.J. Verstegen, A.L.N. Stevel, J. Lumin. 9 (1974) 406.
[42] C.R. Ronda, B.M.J. Smets, J. Electrochem. Soc. 136 (1989) 570.
[43] B. Smets, J. Rutten, G. Hocks, J. Verlijsdon, J. Electrochem. Soc. 136 (1989) 2119.
[44] R. Jagannathan, R.P. Rao, T.R.N. Kutty, Mater. Res. Bull. 27 (1992) 459.
[45] C.N.R. Rao, Chemical Approaches to the Synthesis of Inorganic Materials, Wiley, New Delhi, 1994.
[46] K.G. Broadhead, H.H. Heady, Anal. Chem. 32 (1960) 603.
[47] D.W. Johnson Jr., Ceram. Bull. 60 (1981) 221.
[48] S. Erdei, R. Roy, G. Harshe, H. Juwhari, D. Agarwal, F.W. Ainger, W.B. White, Mater. Res. Bull. 30 (1995) 745.
[49] R.P. Rao, Solid State Commun. 99 (1996) 439.
[50] M.L.F. Phillips, Soc. Photo-Opt. Indust. Eng. 2408 (1995) 200.
[51] R. Roy, D.M. Roy, T.P. O'Holleran, Powder Metal. Intl. 16 (1984) 274.
[52] M.H. Lee, S.G. Oh, S.C. Yi, J. Colloid Interface Sci. 226 (2000) 65.
[53] T. Hirai, Y. Asada, I. Komasawa, J. Colloid Interface Sci. 276 (2004) 339.
[54] P.K. Sharma, M.H. Jilavi, R. Nass, H. Schmidt, J. Lumin. 82 (1999) 187.
[55] J.J. Kingsley, K.C. Patil, Mater. Lett. 6 (1988) 427.
[56] K.C. Patil, S.T. Aruna, S. Ekambaram, Curr. Opin. Solid State Mater. Sci. 2 (1997) 158.
[57] S. Ekambaram, K.C. Patil, Bull. Mater. Sci. 18 (1995) 921.
[58] S. Ekambaram, K.C. Patil, J. Alloys Compd. 217 (1995) 104.
[59] S.S. Trond, J.S. Martin, J.P. Stavanage, A.L. Smith, J. Electrochem. Soc. 116 (1969) 1047.
[60] S. Ekambaram, K.C. Patil, J. Mater. Chem. 5 (1995) 905.
[61] M. Faucher, J. Pannetier, Acta Crystallogr. B36 (1980) 3209.
[62] G. Blasse, A. Bril, W.C. Nieuwpoort, J. Phys. Chem. Solids 27 (1966) 1587.
[63] W. van Schaik, G. Blasse, Chem. Mater. 4 (1992) 410.
[64] A.K. Levine, F.C. Palilla, Electrochem. Technol. 4 (1966) 16.
[65] J.A. Baglio, G. Gashurov, Acta Cryst. B24 (1968) 292.
[66] S. Ekambaram, K.C. Patil, J. Alloys Compd. 248 (1997) 7.
[67] S. Kimura, E. Bannai, I. Shindo, Mater. Res. Bull. 17 (1982) 209.
[68] B. Smets, J. Rutten, J. Hoeks, Verlijsdank, J. Electrochem. Soc. 136 (1989) 2119.
[69] A.L.N. Stevel, J. Lumin. 17 (1978) 12.
[70] F.P.F. van Berkel, H.W. Zandbergen, G.C. Verschoor, D.W. Ijdos, Acta Cryst. C40 (1984) 1124.
[71] G. Blasse, A. Brill, Philips Res. Repts. 23 (1968) 201.
[72] S. Ekambaram, K.C. Patil, J. Mater. Synth. Process. 4 (1996) 337.
[73] M. Gasperin, M.C. Saine, A. Kahn, F. Laville, A. Lejus, J. Solid State Chem. 54 (1984) 61.